

**Design and fabrication of a SAW device with Ta filled microcavities inserted into its delay path for improved power transfer**

Mandek Richardson, Surya Cheemalapati, Richard Everly, Subramanian K. R. S. Sankaranarayanan, Anna Pyayt, and Venkat R. Bhethanabotla

Citation: *Journal of Vacuum Science & Technology B* **33**, 022001 (2015); doi: 10.1116/1.4906515

View online: <http://dx.doi.org/10.1116/1.4906515>

View Table of Contents: <http://scitation.aip.org/content/avs/journal/jvstb/33/2?ver=pdfcov>

Published by the AVS: Science & Technology of Materials, Interfaces, and Processing

---

**Articles you may be interested in**

[Shear-horizontal surface acoustic wave phononic device with high density filling material for ultra-low power sensing applications](#)

*Appl. Phys. Lett.* **104**, 253501 (2014); 10.1063/1.4884655

[Design and fabrication of surface acoustic wave delay line for surface acoustic wave chemical-agent sensors](#)

*J. Vac. Sci. Technol. B* **27**, 1821 (2009); 10.1116/1.3151857

[Focused ion beam etching for the fabrication of micropillar microcavities made of III-V semiconductor materials](#)

*J. Vac. Sci. Technol. B* **25**, 1197 (2007); 10.1116/1.2749528

[Fabrication of InAs quantum dots in Al As/Ga As DBR pillar microcavities for single photon sources](#)

*J. Appl. Phys.* **97**, 073507 (2005); 10.1063/1.1882764

[Fabrication of high Q square-lattice photonic crystal microcavities](#)

*J. Vac. Sci. Technol. B* **21**, 2918 (2003); 10.1116/1.1629298

---



**WE'RE SEARCHING FOR**  
**SKILLED ANTENNA, RF SYSTEMS AND MICROWAVE DESIGN ENGINEERS.**  
HELP US ENGINEER A BETTER TOMORROW. [LEARN MORE](#)

**LOCKHEED MARTIN**

# Design and fabrication of a SAW device with Ta filled microcavities inserted into its delay path for improved power transfer

Mandek Richardson and Surya Cheemalapati

*Department of Chemical and Biomedical Engineering, University of South Florida, 4202 E. Fowler Ave., ENB 118, Tampa, Florida 33620*

Richard Everly

*Nanotechnology Research and Education Center, University of South Florida, 4202 E. Fowler Ave., ENB 118, Tampa, Florida 33620*

Subramanian K. R. S. Sankaranarayanan

*Argonne National Laboratory, Center for Nanoscale Materials, 9700 South Cass Avenue, Building 440, Argonne, Illinois 60439*

Anna Pyayt and Venkat R. Bhethanabotla<sup>a)</sup>

*Department of Chemical and Biomedical Engineering, University of South Florida, 4202 E. Fowler Ave., ENB 118, Tampa, Florida 33620*

(Received 28 August 2014; accepted 12 January 2015; published 30 January 2015)

The authors report the design and fabrication of a surface acoustic wave (SAW) device with improved power transfer due to modification of its delay path. Typically, SAW delay-line devices suffer from relatively high insertion loss (IL) ( $\sim 10\text{--}30$  dB). Our approach is to incorporate an array of microcavities, having square cross-sectional area ( $\lambda/2 \times \lambda/2$ ) and filled with tantalum, within the delay path to maximize acoustic confinement to the surface and reduce IL. To determine the effectiveness of the cavities without expending too many resources and to explain trends found in actual devices, a finite element model of a SAW device with tantalum filled cavities having various depths was utilized. For each depth simulated, IL was decreased compared to a standard SAW device. Microcavities  $2.5\ \mu\text{m}$  deep filled with tantalum showed the best performance ( $\Delta\text{IL} = 17.93$  dB). To validate simulated results, the authors fabricated a SAW device on ST  $90^\circ$ -X quartz with microcavities etched into its delay path using deep reactive ion etching and filled with tantalum. Measurement of fabricated devices showed inclusion of tantalum filled microcavities increased power transfer compared to a device without cavities. © 2015 American Vacuum Society.

[<http://dx.doi.org/10.1116/1.4906515>]

## I. INTRODUCTION

Surface acoustic wave (SAW) devices have been used for decades in the communications field,<sup>1,2</sup> and within the last 15–20 years, they have found frequent use in gas,<sup>3–5</sup> chemical,<sup>6–8</sup> and biosensing applications.<sup>9–13</sup> SAW devices can take the form of a resonator or delay-line. In a delay-line configuration, a pair of interdigital transducers (IDTs) are fabricated on top of a piezoelectric substrate and separated by a predetermined distance.<sup>14</sup> One of the IDTs serves as the device input and the second as the output. Application of an AC voltage to the input IDT generates a wave via the piezoelectric effect. This wave travels along the substrate surface until it reaches the output IDT, where a current is generated and detected via the inverse piezoelectric effect. Typically, SAW delay-line devices suffer from large insertion losses (IL) (10–30 dB).<sup>15</sup> For example, the surface skimming bulk mode of ST-Quartz, measured in air, usually has an IL of 20–30 dB even when a waveguide is applied.<sup>16,17</sup> Such high losses are detrimental in sensing and communication applications. Several methods have been employed to reduce IL such as the fabrication of

metal gratings and grooves,<sup>18–22</sup> application of a waveguide,<sup>23–25</sup> and altering the design of the IDTs to generate unidirectional waves.<sup>26</sup> The types of losses minimized by these methods are those attributed to acoustic wave penetration into the bulk material and bidirectional wave generation by each IDT. In the former case, where acoustic waves are confined more at the surface, there is an increase in sensitivity to surface perturbations. As a result, if used in communication applications, careful consideration must be given to device packaging. This is to avoid unwanted frequency shifts that would occur if interaction with the environment is not limited. In addition, losses caused by surface perturbations could counteract any improvements made from decreasing the IL. On the contrary, increased sensitivity at the surface would be beneficial for sensing applications. Based on the approaches mentioned to decrease IL, an alternative method in which the SAW delay path is modified with an array of microcavities was investigated.<sup>15,27,28</sup> These studies showed that the incorporation of cavities greatly enhance sensor sensitivity to mass loading and power transfer for different piezoelectric substrates (langasite and lithium tantalate). In addition, power transfer and sensitivity are further improved when the cavities are filled with a waveguide material (polystyrene). However,

<sup>a)</sup>Electronic mail: [bhethana@usf.edu](mailto:bhethana@usf.edu)

the realization of actual devices is a challenge due to the difficulties in etching these materials.

There has been success etching various piezoelectric materials with reactive ion etching (RIE).<sup>29–32</sup> RIE is a highly controllable dry etch process, which employs chemical and physical means to achieve anisotropic material removal. Typically, to have a SAW device with low insertion loss, a piezoelectric material with a high electromechanical coupling coefficient ( $k^2$ ) such as lithium niobate and lithium tantalate is necessary. However, the etch rate of these materials is slow when compared to single crystalline quartz, another piezoelectric material, but with a lower  $k^2$  value. This is because the fluorides formed from lithium and tantalum oxides, and niobium oxides are nonvolatile.<sup>30</sup> Thus, to remove these residues requires a lower process pressure, use of a heavier noble gas (i.e., Xe instead of Ar), and an increased RF bias to provide more energy to ions. Under these process conditions, etching occurs more by physical sputtering. Because the reaction products are more volatile, the process parameters can be changed when etching quartz to increase chemical etching. As a result, faster etch rates can be realized.<sup>30,33</sup> Another drawback to etching lithium niobate and lithium tantalate by RIE is since highly energetic ions are needed to bombard the surface, decreased mask selectivity is a factor if using photoresist. It is possible to improve selectivity if a nickel mask is used,<sup>32</sup> but this would increase the complexity and processing steps, which may affect the integrity of the IDT structures present on the wafer. Recently, we performed a study utilizing ST-Quartz substrates modified with microcavities<sup>28</sup> that showed similar findings to the aforementioned investigations done on lithium tantalate<sup>15</sup> and langasite.<sup>27</sup> In this work, simulated devices were easily fabricated due to quartz's faster etch rate and robustness.

To avoid total reflection of the acoustic wave at the microcavity interface as a result of the large acoustic impedance mismatch between air and quartz, a filling material with an impedance value closer to quartz is necessary. Equation (1) shows that acoustic impedance,  $Z$ , is dependent on density ( $\rho$ ) and velocity ( $V$ )

$$Z = \rho V. \quad (1)$$

Since the acoustic impedance of quartz is relatively high ( $Z_{\text{quartz}} = 13.58 \text{ M}\Omega$ ), a material with high density is chosen to increase transmission through the composite structure. In addition, to effectively utilize the waveguiding effect, the material must have an acoustic velocity less than that of quartz (velocity = 5060 m/s). For these reasons, tantalum was chosen as the filling material in this study.

In this work, we describe the fabrication and characterization processes used to insert an array of tantalum filled microcavities within the delay path of a SAW device (Fig. 1). Prior to fabricating any devices, a finite element model (FEM) was utilized to determine cavity effectiveness and to establish trends related to cavity depth on performance ( $\Delta\text{IL}$ ). FEMs are useful for studying complex geometries (i.e., microcavities) and analyzing different design

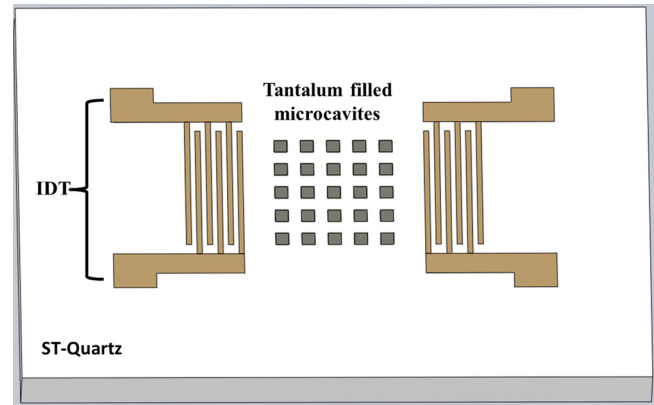


FIG. 1. (Color online) Illustration of a SAW device with tantalum filled microcavities.

variations without having to expend large amount of resources. Many studies of SAW devices and sensors have been completed using FEM to study acoustic wave propagation.<sup>15,27,28,34,35</sup> Similarly, we used FE simulations to gain a physical understanding of how the presence of microcavities affects acoustic wave propagation and how this relates to changes in IL. However, FE modeling of actual SAW devices is computationally intensive and not possible with the computational resources we have at hand. So, the device response due to the addition of cavities cannot be accurately simulated. Thus, we utilized a parametric study of different cavity geometries to explain trends that would be seen in actual devices. Lastly, we measured the frequency response of a fabricated device containing tantalum filled cavities and compared it to the frequency response of a standard SAW delay-line. Our combined experimental and simulation results demonstrate that SAW devices with tantalum filled microcavities can be successfully fabricated and are effective at reducing IL.

## II. FINITE ELEMENT MODEL

A 3D structural FEM was developed in the multiphysics software ANSYS 14.5 to evaluate SAW devices based on ST 90°-X quartz with and without an array of tantalum filled microcavities in the delay path (Fig. 1). Each microcavity has a square cross-sectional area of  $\lambda/2 \times \lambda/2$  ( $\lambda = 40 \mu\text{m}$ ) and a depth of 0.5, 1.0, or 2.5  $\mu\text{m}$ . The SAW device was configured as a two-port delay line in which the substrate length, width, and depth was 1600, 200, and 500  $\mu\text{m}$  respectively. The depth was chosen to represent the thickness of an actual SAW substrate, while the length was chosen to limit the amount of reflections from the substrate edges. Suppression of edge reflections ensures interference with acoustic wave propagation between the input and output IDTs is avoided. Both the input and output IDTs are composed of three finger pairs with a spatial periodicity of 40  $\mu\text{m}$ , finger width of 10  $\mu\text{m}$ , and aperture height of 60  $\mu\text{m}$ . To simplify the analysis, the IDT fingers were defined as massless elements, represented by a set of nodes coupled through the voltage degree of freedom. Thus, second order effects are ignored. The

distance between the IDTs ( $4\lambda$ ) sets the delay path length. The IDT dimensions and delay path length used in the FE model are scaled down from those of a fabricated device to reduce simulation time and computational resources.

The SAW frequency response was obtained by taking the Fourier transform of the impulse response. To obtain the impulse response, an impulse voltage signal, having amplitude of 100 V, is applied to the transmitting IDT. The structure was simulated for 200 ns using a time step of 0.95 ns. After completion of the simulation, the output voltage versus time is taken from a selected node on the output IDT. The voltage versus time data is converted into the frequency response by applying an FFT algorithm using a custom MATLAB code.

### III. EXPERIMENT

#### A. Fabrication of SAW device

SAW devices were fabricated on ST 90°-X quartz wafers, 500  $\mu\text{m}$  thick and 4 in. in diameter. Each SAW device was configured in a delay line setup where each IDT is composed of a single split finger design with a metallization ratio = 0.5. The IDT has periodicity,  $\lambda = 40 \mu\text{m}$ , and aperture height = 50  $\lambda$ . The distance between the input and output IDTs = 200  $\lambda$ . Based on the given IDT periodicity and substrate velocity, the theoretical operating frequency is 126.5 MHz.

To remove contaminants, each wafer was solvent cleaned (acetone, methanol, and isopropyl alcohol), rinsed with DI water, and dried with an  $\text{N}_2$  stream. Excess water/water vapor was removed by placing the wafers on a hotplate for 5 min at 115 °C. Negative tone photoresist, NR9 1500 PY (Futurrex) was applied to the wafer via spin-coating for 40 s at 3000 rpm. This produced a resist thickness of  $\sim 1.6 \mu\text{m}$ . The resist was soft baked on a hotplate for 1 min at 150 °C then left to cool on a metal surface. Next, the resist was exposed to broadband UV light at 20  $\text{mW}/\text{cm}^2$  intensity for 3 s. A subsequent hard bake step (1 min at 100 °C) was followed by immersion of the wafer in an RD6 developer solution for 12 s.

The IDTs were formed via a lift-off procedure. A 200 nm thick aluminum film was e-beam deposited over the entire patterned wafer. Removal of excess metal was accomplished by soaking it in acetone for at least 30 min. To ensure all the metal is removed from between the IDT fingers, the wafer was ultrasonicated in acetone for 30–60 s.

#### B. Etching and filling of microcavities

The etching of microcavities was performed in a deep reactive ion etching (DRIE) system (Adixen AMS 100 DRIE). Several masking materials have been employed for the dry etching of quartz/glass substrates. These include Si, Ni, and SU8.<sup>36</sup> For this work, we used a positive tone photoresist, AZ4620 (Clariant). This resist offers good selectivity and is easier to implement and remove compared to a Si or Ni mask. After patterning the wafer with the SAW die, AZ4620 was applied during a second lithography step forming an etch mask for the array of microcavities in the area between the IDTs. To increase the durability of the resist, it was cured

in an oven for 4 h at 70 °C. This temperature was chosen to prevent reflow of the resist and distortion of the cavity features. Before the microcavities can be etched, the wafer was diced into individual dies. Attempts were made to etch at the wafer scale. However, due to the pyroelectric effect, the wafers bowed considerably when heated. This phenomenon caused a loss of thermal contact with the substrate holder and an accumulation of stress. As a result, wafers broke during our initial attempts at processing devices. Thus, by etching at the die level, the surface area was reduced enough to eliminate the problem. The pump maintained a chamber pressure of 1.1 Pa, with process gases  $\text{C}_4\text{F}_8$ ,  $\text{O}_2$ , and He was constantly input into the system. Table I shows the etch parameters used in the process.

After etching, the devices were placed in  $\text{O}_2$  plasma at low RF power (50 W) and a flow rate of 350 sccm for 3 min to remove any photoresist that may have redeposited on the bottom cavity surface. The photoresist is left on and doubles as a lift-off mask for the deposition and removal of excess tantalum. Tantalum was deposited using e-beam, and lift-off was performed by placing the chips in acetone for approximately 30 min. The entire process is outlined in Fig. 2.

#### C. Characterization of etching process

Characterization of the DRIE process was accomplished by using profilometer measurements in conjunction with SEM. To determine the etch rate and mask selectivity, we made three separate measurements with an alphastep profilometer on several devices before filling the cavities with tantalum. The first measurement was conducted prior to etching the substrate to determine the thickness of the mask. The second measurement was performed after etching with DRIE and before removing the photoresist mask. The last measurement was taken after the resist was stripped from the wafer. During etching, issues such as microtrenching and micromasking can result that may affect fabrication and device performance. To verify if these issues are present and to ensure the cavities were filled with tantalum, we monitored the different stages of fabrication with a HITACHI SU-70 SEM.

#### D. Measurement of frequency response

Comparison of a SAW device with and without microcavities included in the delay path was carried out using a network analyzer (Agilent 8753 ES). The devices were inserted in a custom-made test cell and IL versus frequency was

TABLE I. DRIE process conditions.

Chamber pressure	1.1 Pa	
Process gas mixture		
$\text{CH}_4$	He	$\text{C}_4\text{F}_8$
13.0 sccm	149.7 sccm	17.0 sccm
Bias power	400 W	
Source RF power	2800 W	
Substrate temperature	−20 °C	
Distance to target	140 mm below plasma source	

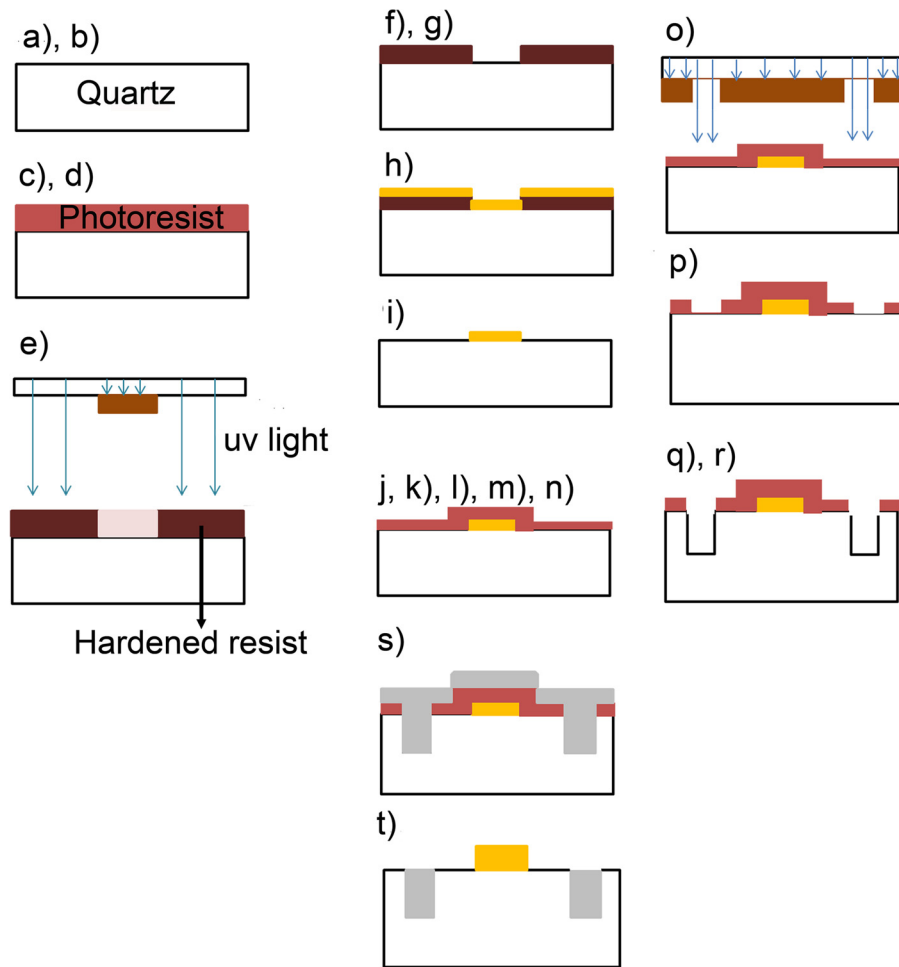


FIG. 2. (Color online) Process flow for fabricating Ta filled microcavities: (a) solvent clean wafer with acetone, methanol, and isopropyl alcohol, rinse with DI water, and dry with  $N_2$  stream; (b) dehydration bake in oven or on hotplate; (c) spin on NR9 1500PY photoresist; (d) softbake in oven at  $120^\circ C$  for 10 min; (e) expose with broadband UV light with Karl Suss Mask Aligner; (f) hard bake in oven at  $100^\circ C$  for 15 min; (g) develop in RD6 for 12 s; (h) deposit Ti/Au via e-beam evaporator; (i) lift-off photoresist and excess metal; (j) clean wafer with  $O_2$  plasma for 5 min; (k) solvent clean similar to step (a); (l) apply HDMS to the wafer surface; (m) apply AZ4620 photoresist; (n) soft bake in oven for 20 min in oven at  $95^\circ C$ ; (o) expose with broadband UV light with Karl Suss mask aligner; (p) develop resist in 1:4 AZ 400 K developer for 4 min; (q) dice wafer into individual die; (r) etch quartz using DRIE; (s) deposit tantalum; and (t) remove photoresist.

obtained. To get rid of spurious signals such as triple transit and electromagnetic feedthrough, the time gating option was applied.

## IV. RESULTS AND DISCUSSION

### A. Simulation results

The figure of merit utilized in this study to show the effect of inserting microcavities into the delay path is IL. In Fig. 3, the simulated frequency response for the substrate without microcavities is compared to several devices having microcavities filled with tantalum of various depths. The center frequency and IL for the standard SAW delay-line device was 129.2705 MHz and  $-38.17$  dB. Analysis of the frequency response shows that employing filled microcavities of any depth within the SAW delay path reduces IL with the largest reduction occurring for microcavities  $2.5 \mu m$  deep ( $\Delta IL = 17.93$  dB). In addition to increasing power transfer, further inspection of the plot shows that the SAW pass-band is narrowed, power is increased for higher frequency wave

modes, and there is an upward shift of the fundamental frequency due to an apparent increase in the acoustic velocity of the fundamental wave mode. Simulated IL and center frequency results are given in Table II.

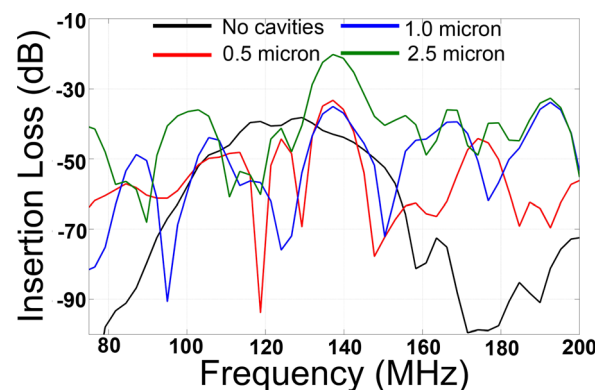


FIG. 3. (Color online) Plot of IL vs frequency for SAW devices with Ta filled microcavities having depths of 0.5, 1.0, and  $2.5 \mu m$  and a device without microcavities within the delay path.

TABLE II. Simulated results for IL and center frequency for the various SAW device configurations.

Microcavity depth ( $\mu\text{m}$ )	IL (dB)	$\Delta\text{IL}$ (dB)	$f_0$ (MHz)	$\Delta f_0$ (MHz)
0.5	-33.25	4.92	137.1851	7.91
1.0	-33.82	4.36	192.5867	63.2
2.5	-20.24	17.93	137.1851	7.91

To explain the decrease in IL,  $x$ ,  $y$ , and  $z$  displacements versus time for a node on the output IDT were plotted and are shown in Fig. 4. For a shear-horizontally (SH) polarized SAW, primary displacement would occur in the  $x$ -direction, which is perpendicular to the direction of wave propagation and parallel to the surface. The displacements plotted in Fig. 4(a) are evidence that the SAW has SH polarization. When microcavities are inserted into the SAW delay path, displacements are increased in all three directions, by two orders of magnitude, with respect to the standard SAW device, which explains the decrease in IL. Another conclusion that can be drawn from the displacement plots is the underlying cause for the upward shift in center frequency. Unlike the results of Fig. 4(a), displacements in the  $y$  and  $z$ -directions are not insignificant with respect to  $x$ -displacements for the SAW devices with microcavities. Displacements that occur in this direction are characteristic of longitudinal and shear-vertical bulk waves. Our results show that the presence of microcavities causes reflection and confinement of bulk waves to the surface, which contribute to the excitement of the output IDT. Since these bulk waves travel at a higher velocity than the fundamental wave mode, constructive interference results in a positive shift of the center frequency.

## B. Fabrication results

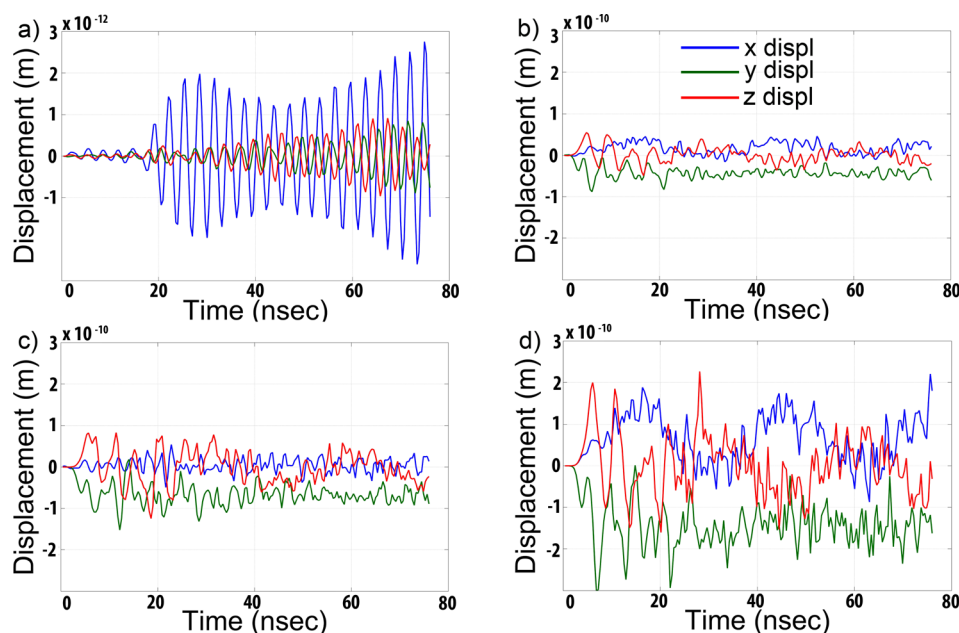
SAW devices containing Ta filled microcavities were successfully fabricated on ST 90°-X quartz substrates. The

TABLE III. Measurement results used to determine material etch rate and mask selectivity.

Process layer and step	Average thickness ( $\mu\text{m}$ )
Photoresist no etching	$9.915 \pm 0.0397$
Photoresist + etched substrate	$13.063 \pm 0.065$
Etched substrate	$6.503 \pm 0.0115$

process flow is shown in Fig. 2. To determine the time needed to etch microcavities of a desired depth in quartz, we ran several trials. These trials were used to figure out the etch rate of the photoresist and substrate, and with this information, we calculated mask selectivity. Prior to placing the devices into the DRIE chamber, we cured the photoresist to increase its resistance to etching. Optimized results were achieved when the resist was cured for at least 2–4 h at a moderately low temperature (i.e., 50–70°C). As a result, reflow can be controlled enough to prevent distortion of the features and the selectivity was improved. There are three key profilometer measurements needed for the etch rate calculations. The first measurement is made prior to etching to determine the thickness of the resist. A second measurement is taken after DRIE and before the resist is stripped by soaking in acetone. The third and final measurement is made after the resist is removed and is used to determine the etch rate of quartz. The photoresist etch rate can be found by subtracting the third measurement from the second measurement to yield the amount of photoresist left. This value is subtracted from the initial thickness to give the amount of resist etched. The measured results after each step can be found in Table III.

The amount of material etched was determined after the devices were in the chamber for 10 min. Based on data from Table III, the quartz etch rate is 5419 Å/min, the photoresist etch rate is 3355 Å/min, and the selectivity is 1.62.

FIG. 4. (Color online) Plot of  $x$ ,  $y$ , and  $z$ -displacements vs time for a SAW device with (a) no cavities, (b) 0.5  $\mu\text{m}$ , (c) 1.0  $\mu\text{m}$ , and (d) 2.5  $\mu\text{m}$  deep cavities.

Each etched device contains microcavities with a depth of  $0.5\ \mu\text{m}$ . This ensures that a large ratio exists between photoresist thickness and metal thickness. This was necessary in order to perform lift-off with a positive tone resist that does not have a re-entrant profile after its development. The four stages involved in fabricating the microcavity structures and filling them with tantalum were closely monitored at every step using SEM. The results are presented in Fig. 5. All samples were sputter coated with gold/palladium films a few nanometers thick to improve SEM imaging because the substrate (ST-Quartz) is a dielectric with low conductivity. Sample images were taken while positioned at a  $45^\circ$  angle. This allowed the visualization of the sidewalls and interior of the cavities since a traditional approach of cutting the wafer with a diamond scribe was not possible due to the large tip size compared to the cross-sectional area of the microcavities. Figure 5(a) shows a smooth and vertical photoresist profile after photolithography, which is important to effectively etch anisotropic structures into quartz. After etching, the integrity of the photoresist has been maintained [Fig. 5(b)] because a low temperature-curing step for AZ4620 photoresist was employed. An image taken upon removal of the photoresist [Fig. 5(c)] shows uniform etching across the cavity with low surface roughness. The final image is taken after the cavity has been filled with tantalum, and the photoresist has been removed [Fig. 5(d)]. The image shows complete filling of the cavity, but a metal film has accumulated along the perimeter adding unwanted topography to the surface. The nonuniform surface will adversely affect SAW propagation. However, this residual material can easily be removed by mechanical polishing.

The process presented to fabricate SAW devices with tantalum filled microcavities only requires two lithography steps. For this reason, the process is competitive with that

required to apply a waveguide material, which is the method most frequently used to decrease the IL of SH-SAWs. In addition, the etch rates from device to device have a standard deviation of  $\pm 11.5\ \text{nm}$  (Table III). This also makes the process competitive with methods usually employed to deposit various waveguide materials [i.e., sputtering or plasma enhanced vapor deposition (PECVD)]. However, in our facility, the DRIE chamber can only handle one wafer at a time. Whereas the PECVD chamber can handle up to six to ten wafers, depending on wafer diameter, thus, throughput is substantially greater. It is possible to use a similar sized chamber where RIE is employed. However, because of the lower RF bias power available, etching time is increased by a factor of 2. This may not be a problem if the times for waveguide deposition and etching are similar.

### C. Insertion loss measurements

Assessment of microcavity effectiveness was accomplished by measuring the IL of a standard SAW delay line device and comparing it to a device augmented with tantalum filled cavities having a depth of  $0.5\ \mu\text{m}$  (Fig. 6). Spurious responses due to electromagnetic feed through, triple transit reflections, and bulk waves appearing at the output IDT were eliminated by employing the time gating option on the network analyzer. The aforementioned frequency response measurements show tantalum filled microcavities reduced IL by 7.615 dB (Fig. 6). Qualitatively, this is consistent with our simulations. However, the improvement in power transfer is larger than what was obtained through simulations ( $\Delta\text{IL} = 4.95\ \text{dB}$ ). There are two reasons for this discrepancy. First, because a FE model of a complete SAW device is computationally intensive and not possible even with the present computational resources, the model

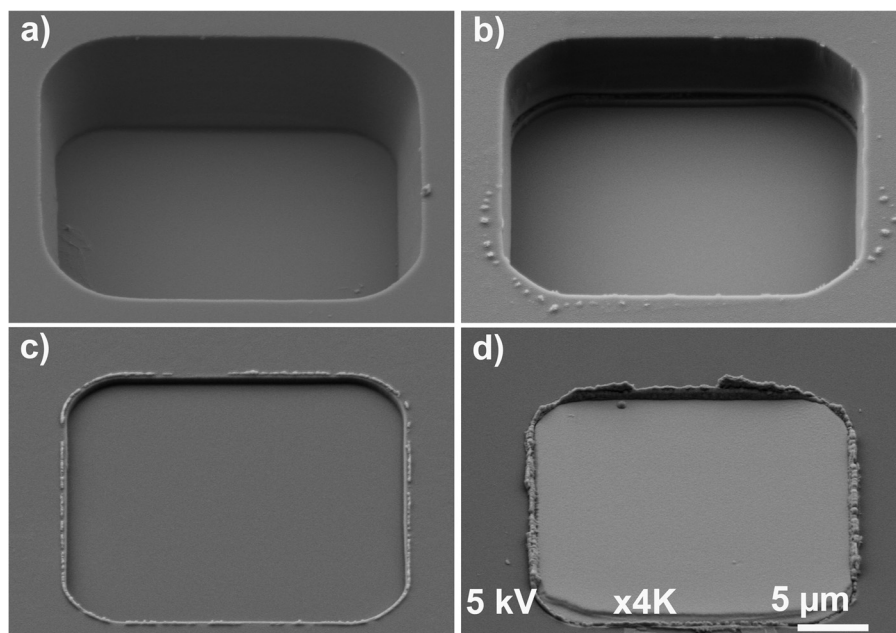


Fig. 5. SEM images showing (a) the patterned photoresist, (b) a profile view after etching and with photoresist remaining (c) a profile view after etching with photoresist removed, and (d) the etched cavities filled with metal.

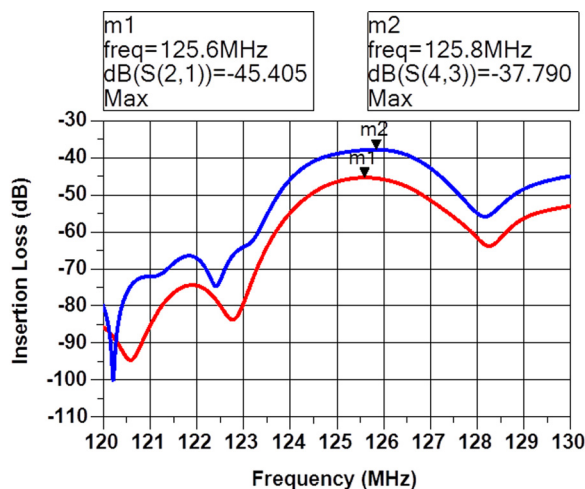


Fig. 6. (Color online) Comparison of the measured frequency responses for a standard SAW delay line device vs a SAW delay line device with Ta filled cavities included in the delay path (m1 is the marker indicating the IL value at the center frequency of the device containing no cavities and m2 is the marker indicating the IL value at the center frequency for the device with tantalum filled cavities in the delay path).

dimensions are scaled down compared to the actual device. This decreases the number of nodes and finite elements required, which reduces the simulation time and computational resources. However, simulation accuracy is compromised. Second, resistive losses and parasitics that occur from the measurement setup are not accounted for. Therefore, to get an accurate device response a de-embedding procedure is required or an equivalent circuit model must be integrated with the FE simulations to account for the various parasitic effects. Figure 6 also shows that adding tantalum filled cavities increases the center frequency, which is consistent with simulations. However, the change in frequency is a factor of 40 smaller than what was seen in simulations. Since the simulated devices only contain 3 IDT finger pairs compared to 60 finger pairs in the fabricated device, a broader pass band is expected. Therefore, inferring accurate frequency shifts for simulated devices is difficult. As a result, a direct comparison between simulations and experiment is not possible at this time. It is possible to simulate devices with several tens of finger pairs which would result in a pass band narrow enough to indentify small shifts in frequency. However, simulation time and computational resources would be greatly increased. At this point, our study is concerned only with determining possible trends with respect to  $\Delta$ IL when microcavities are added.

In conclusion, future work is underway to fabricate devices with  $2.5 \mu\text{m}$  cavities to see if we can get close to the large increase in power transfer shown in simulations ( $\Delta$ IL = 17.93 dB). In addition, we are working on getting closer agreement between experiments and simulations.

## V. SUMMARY AND CONCLUSIONS

We have successfully fabricated a SAW device containing tantalum filled microcavities within its delay. Prior to device fabrication a FEM was used to determine if inserting microcavities will decrease IL and to establish if any trends

exists between cavity depth and improved power transfer. Our simulations show that for each depth (0.5, 1.0, and  $2.5 \mu\text{m}$ ) IL is decreased compared to a standard SAW device. The largest decrease occurs when the cavity depth is  $2.5 \mu\text{m}$  ( $\Delta$ IL = 17.93 dB). Next, devices with  $0.5 \mu\text{m}$  deep microcavities filled with tantalum were fabricated. To etch cavities into the substrate, DRIE was used. The etch rate we obtained was  $5419 \text{ \AA}/\text{min}$ , which is comparable to rates found in the literature.<sup>37–39</sup> SEM was used to characterize the etching process. The images acquired with SEM show low surface roughness and vertical sidewalls, which are vital for SAW propagation. The fabrication procedure presented only requires two lithography steps, which make it comparable to applying a waveguide with respect to processing steps. Lastly, the effect on device performance was determined by comparing the measured frequency responses of SAW devices with and without microcavities. Experimental results show that tantalum filled cavities reduced IL by 7.615 dB. The simulated device having the same depth only shows a  $\Delta$ IL = 4.95 dB. Discrepancy between simulations and experiment are due to the size difference between the model and actual device, and parasitic effects resulting from the measurement setup. The FE model of the SAW device is reduced in size compared to a real SAW device due to the large amount of computational resources that would be required to simulate an actual device. As a result, the actual device response cannot be simulated accurately, so we rely on the FE model to explain trends. In conclusion, both simulations and experiments show that power transfer can be greatly enhanced by inserting tantalum filled cavities into a SAW delay path. Future work is needed to obtain closer agreement between simulated and experimental devices. Our proposed device will be useful in remote sensing and communication applications that require SAW delay line devices because of its decreased power consumption.

## ACKNOWLEDGMENTS

The authors would like to thank the Research Computing, within USF Information Technology, University of South Florida for use of software and access to high performance computing resources. The authors would also like to thank the staff at USF's Nanomanufacturing Research and Education Center (NREC). Use of the Center for Nanoscale Materials is supported by the U.S. Department of Energy, Office of Science, Office of Basic Energy Sciences, under Contract No. DE-AC02-06CH11357.

- <sup>1</sup>R. Weigel, D. P. Morgan, J. M. Owens, A. Ballato, K. M. Lakin, K.-y. Hashimoto, and C. C. W. Ruppel, *IEEE Trans. Microwave Theory Tech.* **50**, 738 (2002).
- <sup>2</sup>C. C. W. Ruppel, L. Reindl, and R. Weigel, *IEEE Microwave Mag.* **3**, 65 (2002).
- <sup>3</sup>W. Wen, H. Shitang, L. Shunzhou, L. Minghua, and P. Yong, *Sens. Actuators, B* **125**, 422 (2007).
- <sup>4</sup>J. A. Thiele and M. P. da Cunha, *Sens. Actuators, B* **113**, 816 (2006).
- <sup>5</sup>M. Penza, P. Aversa, G. Cassano, W. Wlodarski, and K. Kalantarzadeh, *Sens. Actuators, B* **127**, 168 (2007).
- <sup>6</sup>A. J. Ricco, R. M. Crooks, and G. C. Osbourn, *Acc. Chem. Res.* **31**, 289 (1998).

- <sup>7</sup>M. Rapp, J. Reibel, A. Voigt, M. Balzer, and O. Bülow, *Sens. Actuators, B* **65**, 169 (2000).
- <sup>8</sup>F. Josse, F. Bender, and R. W. Cernosek, *Anal. Chem.* **73**, 5937 (2001).
- <sup>9</sup>B. E. Rapp, F. J. Gruhl, and K. Länge, *Anal. Bioanal. Chem.* **398**, 2403 (2010).
- <sup>10</sup>M.-I. Rocha-Gaso, C. March-Iborra, A. Montoya-Baides, and A. Arnau-Vives, *Sensors* **9**, 5740 (2009).
- <sup>11</sup>E. Berkenpas, P. Millard, and M. Pereira da Cunha, *Biosens. Bioelectron.* **21**, 2255 (2006).
- <sup>12</sup>D. W. Branch and S. M. Brozik, *Biosens. Bioelectron.* **19**, 849 (2004).
- <sup>13</sup>T. M. Gronewold, *Anal. Chim. Acta* **603**, 119 (2007).
- <sup>14</sup>R. M. White and F. W. Voltmer, *Appl. Phys. Lett.* **7**, 314 (1965).
- <sup>15</sup>S. Cular, S. K. R. S. Sankaranarayanan, and V. R. Bhethanabotla, *Appl. Phys. Lett.* **92**, 244104 (2008).
- <sup>16</sup>D. D. Deogagkar, V. Limaye, S. Sinha, and R. D. S. Yadava, *Sens. Actuators, B* **104**, 85 (2005).
- <sup>17</sup>E. Gizeli, F. Bender, A. Rasmusson, K. Saha, F. Josse, and R. Cernosek, *Biosens. Bioelectron.* **18**, 1399 (2003).
- <sup>18</sup>B. Auld and J. Gagnepain, *Electron. Lett.* **12**, 650 (1976).
- <sup>19</sup>P. D. Bloch, E. G. S. Paige, and L. Solymar, *IEEE Ultrason. Symp.* **1978**, 639.
- <sup>20</sup>V. I. Cherednik and M. Y. Dvoesherstov, *Acoust. Phys.* **56**, 37 (2010).
- <sup>21</sup>K.-Y. Hashimoto, M. Yamaguchi, and H. Kogo, *Electron. Commun. Jpn. Pt. II* **69**, 42 (1986).
- <sup>22</sup>J. Melngailis and R. Williamson, *IEEE Ultrason. Symp.* **1978**, 623.
- <sup>23</sup>J. Du, G. L. Harding, J. A. Ogilvy, P. R. Dencher, and M. Lake, *Sensor Actuators, A* **56**, 211 (1996).
- <sup>24</sup>E. Gizeli, A. C. Stevenson, N. J. Goddard, and C. R. Lowe, *IEEE Trans. Ultrason. Ferroelectr. Freq. Control* **39**, 657 (1992).
- <sup>25</sup>G. Kovacs, G. W. Lubking, M. J. Vellekoop, and A. Venema, *IEEE Ultrason. Symp.* 1992, 281.
- <sup>26</sup>K. Yamanouchi and H. Furuyashiki, *Electron. Lett.* **20**, 989 (1984).
- <sup>27</sup>R. Singh, S. K. R. S. Sankaranarayanan, and V. R. Bhethanabotla, *Appl. Phys. Lett.* **95**, 034101 (2009).
- <sup>28</sup>M. Richardson, S. K. R. S. Sankaranarayanan, and V. R. Bhethanabotla, *Appl. Phys. Lett.* **104**, 253501 (2014).
- <sup>29</sup>Z. Ren, P. J. Heard, J. M. Marshall, P. A. Thomas, and S. Yu, *J. Appl. Phys.* **103**, 034109 (2008).
- <sup>30</sup>P. W. Leech, *J. Vac. Sci. Technol., A* **16**, 2037 (1998).
- <sup>31</sup>S. Schreiter and H. U. Poll, *Sens. Actuators, A* **35**, 137 (1992).
- <sup>32</sup>S. Benchabane, L. Robert, J. Y. Rauch, A. Khelif, and V. Laude, *J. Appl. Phys.* **105**, 094109 (2009).
- <sup>33</sup>Ch. Steinbrüchel, *J. Electrochem. Soc.* **132**, 180 (1985).
- <sup>34</sup>S. Ippolito, K. Kalantar-Zadeh, D. A. Powell, and W. Wlodarski, *IEEE Ultrason. Symp.* **2003**, 303.
- <sup>35</sup>M. Z. Atashbar, B. J. Bazuin, M. Simpeh, and S. Krishnamurthy, *Sens. Actuators, B* **111–112**, 213 (2005).
- <sup>36</sup>H. Chen and C. Fu, *J. Micromech. Microeng.* **18**, 105001 (2008).
- <sup>37</sup>S. Queste, E. Courjon, G. Ulliac, R. Salut, V. Petrini, and J. Rauch, "Deep reactive ion etching of quartz, lithium niobate and lead titanate," *JNTE Proceedings*, Toulouse, France, 2008.
- <sup>38</sup>T. Abe and M. Esashi, *Sens. Actuators, A* **82**, 139 (2000).
- <sup>39</sup>V. N. Hung, T. Abe, P. N. Minh, and M. Esashi, *Sens. Actuators, A* **108**, 91 (2003).